UCLA
UCLA Previously Published Works

Title
Atomically Dispersed Pt1–Polyoxometalate Catalysts: How Does Metal–Support Interaction Affect Stability and Hydrogenation Activity?

Permalink
https://escholarship.org/uc/item/3nn6n3gm

Journal
Journal of the American Chemical Society, 141(20)

ISSN
0002-7863

Authors
Zhang, Bin
Sun, Geng
Ding, Shipeng
et al.

Publication Date
2019-05-22

DOI
10.1021/jacs.9b00486

Supplemental Material
https://escholarship.org/uc/item/3nn6n3gm#supplemental

Peer reviewed

Atomically Dispersed Pt₁-Polyoxometalate Catalysts: How Does Metal-support Interaction Affect Stability and Hydrogenation Activity?

Bin Zhang,[†,#] Geng Sun,[‡,#] Shipeng Ding,[†,#] Hiroyuki Asakura,[∥] Jia Zhang,[⊥] Philippe Sautet,[*,‡,§] and Ning Yan[*,†]

[†]Department of Chemical and Biomolecular Engineering, National University of Singapore, 4 Engineering Drive 4, 117585 Singapore

[‡]Department of Chemical and Biomolecular Engineering, University of California, Los Angeles, Los Angeles, California 90095, United States

[§]Department of Chemistry and Biochemistry, University of California, Los Angeles, Los Angeles, California 90095, United States

[∥]Elements Strategy Initiative for Catalysts & Batteries (ESICB), Kyoto University, Kyoto 615-8245, Japan

[⊥]Institute of High Performance Computing, Agency for Science, Technology and Research 1 Fusionopolis Way #16-16 Connexis, 138632, Singapore.

Abstract

Unlike nano-structured metal catalysts, supported single-atom catalysts (SACs) contain only atomically dispersed metal atoms hinting at much more pronounced metal-support effects. Herein, we take a series of polyoxometalates supported Pt catalysts as examples to quantitatively investigate the stability of Pt atoms on oxide supports and how the Pt-support interaction influences the catalytic performance. For this entire series, we show that the Pt atoms prefer to stay at a four-fold hollow site of one polyoxometalate molecule, and that the least adsorption energy to obtain sintering resistant Pt SACs is 5.50 eV, which exactly matches the cohesive energy of bulk Pt metal. Further, we compared their catalytic performance in several hydrogenation reactions and simulated the reaction pathways of propene hydrogenation by density functional theory calculations. Both experimental and theoretical approaches

suggest that despite the Pt$_1$-support interactions being different, the reaction pathways of various Pt1-polyoxometalate catalysts are very similar and their effective reaction barriers are close to each other and as low as 24 kJ/mol, indicating the possibility of obtaining SACs with improved stability without compromising activity. DFT calculations show that all reaction elementary steps take place only on the Pt atom without involving neighboring O atoms, and that hydrogenation proceeds from the molecularly adsorbed H$_2$ species. Pt-SAC give a weaker H$_2$ adsorption energy than Pt clusters or surfaces, resulting in small adsorption equilibrium constants and small apparent activation barriers which agree between experiment and theory.

Introduction

Supported noble metal catalyst is one of the key classes of current heterogeneous catalysts that are widely applied in industry. The electronic and geometric interactions between metals and supports play a significant role in determining the catalytic performance. Extensive studies have been performed on the interplay between metal nanoparticles (NPs) and oxide supports, revealing that such interactions not only help prevent metal NPs against aggregation by acting as coordinating ligands, but also alter the catalytic properties through charge transfer.[1-5] In recent years, supported metal single-atom catalysts (SACs) containing only atomically dispersed metal atoms with associated neighboring atoms from the support as the catalytically active sites, have received considerable attention because of the unique structural and electronic properties.[6-15] Compared to NPs, isolated atoms are less stable, tending to sinter or agglomerate either by particle coalescence or by Ostwald ripening.[16-17] Interaction between metal atoms and supports is a critical parameter determining stability and activity. Metal atoms with strong binding to supports are resistant to aggregations but may become less reactive,[2, 18] while weaker binding generally implies the risk of sintering at high reaction temperatures. Thus, appropriate selection of metals and supports, as well as rational understanding of the interaction between

2

them, are the keys to prepare SACs with high stability and excellent catalytic performance.

During the past years, supported metal SACs have been successfully applied to various catalytic processes, such as CO oxidation,[19-22] alkene hydroformylation,[23-24] water gas shift reaction,[7, 25-26] methane conversion,[27-28] C-C coupling[29-31], reduction of various functional groups,[32-35] and so on. Among these, catalytic hydrogenation reactions are widely investigated, showing that SACs in a number of cases excel traditional NP catalysts both in activity and selectivity. For instance, the turnover frequency (TOF) of Pd SACs loaded on TiO_2 exceeded the commercial Pd/C catalyst by a factor of 55 and 9 for benzaldehyde and styrene hydrogenation, respectively,[36] while iron oxides supported Pt SACs are highly selective in converting a series of nitroarenes into the corresponding amino products without hydrogenating the substituted groups.[8] In addition, C_3N_4 and graphene supported Pd SACs and mesoporous Al_2O_3 supported Pt SACs are efficient in transforming 1,3-butadiene selectively to alkenes on graphene or carbon nitride.[37-39] Density functional theory (DFT) calculations are employed to explain the superior catalytic performance of some SAC systems. However, most SACs use metal oxide as supports, resulting in a heterogeneous distribution of metal atoms with varied coordination environment due to the non-uniform nature of the support. This may lead to different reaction pathways and/or activities on different sites preventing accurate DFT modelling and rational understanding of the structure-activity correlations.

To date, several issues that are critical for the rational design of SACs remain elusive. For instance, is there a quantitative relation between metal-support interaction and the stability of SACs? In another word, would we be able to predict the possibility of obtaining a reasonably stable SAC for a given metal and support combination? How is H_2 activated on the metal center? What is the species involved in the C-H bond formation step during hydrogenation? H_2 adsorption on metal NPs is dissociative leading to separated H atoms interacting with different neighboring metal atoms,[40-43] but this is obviously not applicable to SACs because metal atoms

3

are spatially separated from each other. Instead, it is proposed in the literature that H_2 undergoes a heterolytic cleavage with one atom on metal center and the other one on the support,[36] but the possibility of homolysis of H_2 on one metal atom, which is commonly seen in homogeneous catalysis,[44] has not been thoroughly considered. It is also unclear whether the strength of metal-support interaction would affect the reaction pathway and the activation energy. A rule of thumb in heterogeneous catalysis is that the increased stability would induce decreased catalytic activity. Is this necessarily true for SACs?

It is not easy to generate a clear or a clearer picture using the myriad of SACs reported in the literature, for which many factors affecting catalytic properties entangle with each other making it challenging to conceive generalizable information. Due to the vastly different synthetic conditions and supports used, the activity of SACs even based on the same metal is not comparable. While Zheng et al found that Pd_1/TiO_2 is far more efficient than traditional Pd NP catalysts in styrene hydrogenation, another report suggests that Pd_1/graphene has poor performance in the same type of reactions. As such, a series of SACs based on uniform, structurally well-defined supports is desirable to resolve some of the critical issues mentioned above. Recently, phosphomolybdic acid (PMA, H_3PMoO_{40}) bearing a Keggin structure has proven to be effective in stabilizing single Pt metal atoms.[45] Considering that quite a few polyoxometalates share the same structure, they offer an ideal platform to study the structure-activity relationship of SACs. [45-47] In the present study, a series of Keggin-structure polyoxometalates dispersed on activated carbon are utilized to stabilize Pt SACs, based on which the boundary condition to prepare Pt_1 SACs instead of forming Pt NPs is identified. The coordination details of Pt_1 on polyoxometalates were elucidated by X-ray absorption fine structure (EXAFS) spectroscopy and DFT calculations. The catalytic performance of different Pt catalysts in several hydrogenation reactions was explored to investigate how supports influence the reactivity of SACs. DFT calculations show that all the elementary steps of

propene hydrogenation take place only on the Pt atom without involving neighboring O atoms, and that the species involved in C-H bond formation is coordinated H_2 and not H, which is different from the previously reported hydrogenation reactions over metal surfaces. DFT simulated effective reaction barriers are consistent with experimental measured activation energies, which are as low as 24 kJ/mol, demonstrating effective SACs system for hydrogenation reactions regardless of the metal-support interaction strength.

Results and Discussion

Catalyst preparation and characterization

Phosphomolybdic acid ($H_3PMo_{12}O_{40}$, PMA), phosphotungstic acid ($H_3PW_{12}O_{40}$, PTA), silicomolybdic acid ($H_4SiMo_{12}O_{40}$, SMA) and tungstosilicic acid ($H_4SiW_{12}O_{40}$, STA) are the four most commonly utilized polyoxometalates with Keggin structure. Additionally all of them have been loaded onto supports as heterogeneous catalysts in previously studies.[34, 48-52] The oxygen-enriched Keggin structure endows each polyoxometalate molecule various anchoring sites for metal atoms with different coordinating environment.[45] However, provided that each metal atom interacts with one polyoxometalate by staying on the most stable site, polyoxometalate offers a good platform for designing SACs with uniform structure. The polyoxometalates are spread onto activated carbon (AC, which is efficient in polyoxometalate adsorption, Figure S1) via wet-impregnation, followed by loading the Pt precursor (platinum acetylacetone, $Pt(acac)_2$) onto the supported polyoxometalates. 0.5 wt% Pt/AC catalyst without polyoxometalates was prepared as a control sample. To preserve the intact structures of polyoxometalates, both the catalyst preparation temperature and catalytic reaction temperature were kept below 200 °C, as confirmed with TGA and TPR results of different polyoxometalates/AC (Figure S2 and Figure S3). The molar ratio of Pt to polyoxometalate is kept as 0.95:1 to constitute pairs containing one Pt atom and one polyoxometalate molecule. To ensure that the acac⁻ ligand was completed removed while agglomeration of Pt atoms were

minimized, the reduction temperature was screened using pre-catalyst (Pt(acac)$_2$-PMA/AC) in the diluted H$_2$ flow at different temperatures (130 to 180 °C). The surface dispersion (ratio of surface atom number to the total atom number) of Pt was derived using H$_2$-O$_2$ titration approach. Polyoxometalate/AC and AC exhibited no hydrogen consumption, and thus the H$_2$ uptake is only determined by Pt species. The samples reduced at 160 to 170 °C prove to have the highest dispersion of ~90% (Table S1), suggesting that the majority of Pt atoms are exposed on the surface, which is as expected for SACs. Since the Pt dispersion decreased dramatically with higher temperature, 160 °C was selected as the reduction temperature. As shown in Figure 3, the Pt dispersion of Pt-SMA/AC and Pt-STA/AC are similar with that of Pt-PMA/AC, hinting that Pt may be atomically dispersed. In contrast, the Pt dispersion for Pt-PTA/AC is only 29.5%, a common value for Pt NPs, indicating the formation of NPs. From ICP-OES analysis (Table S2), the Pt loadings for all the samples are around 0.9 wt%: Pt-PMA/AC (0.88 wt%), Pt-SMA/AC (0.89 wt%), Pt-PTA/AC (0.84 wt%) and Pt-STA/AC (0.85 wt%). In ATR-IR spectra (Figure 1a, b), the peak located at ~1520 cm^{-1}, which is an indicator of the acac$^-$, disappeared from all the catalysts after reduction. Meanwhile, in IR spectra of Pt-polyoxometalate/AC and Pt(acac)$_2$-polyoxometalate/AC materials, characteristic bands for the polyoxometalates in the range of 800-1100 cm^{-1} remain unchanged (ATR-IR results of standards are listed in Figure S4, S5) suggesting the Keggin structure was well preserved during synthesis.

TEM images and XRD patterns were examined to demonstrate whether Pt NPs were formed. Pt NPs with an average size of 1.9 nm were detected in Pt-PTA/AC(Figure 2), and 0.5Pt/AC (Figure S6, S7) but not in the three other samples. EDX analyses (Figure S8, Table S3) over these images showed that the Pt loading in the provided area are all around 0.9 wt%, suggesting that the sizes of Pt species in the three samples are below the detecting limit of TEM (1 nm). In XRD patterns (Figure S9), no reflections corresponding to the characteristic planes of Pt were observed, confirming that the size of the Pt species are below 3 nm. In addition, no

polyoxometalate aggregates were found in TEM images and no characteristic reflections corresponding were detected in XRD patterns (Figure S9, S10), suggesting good dispersion of polyoxometalate molecule. These results match well with H_2-O_2 titration results, consolidating the assumption that Pt keeps single-atom identity in Pt-PMA/AC, Pt-SMA/AC and Pt-STA/AC, and stay in the form of NPs in Pt-PTA/AC.
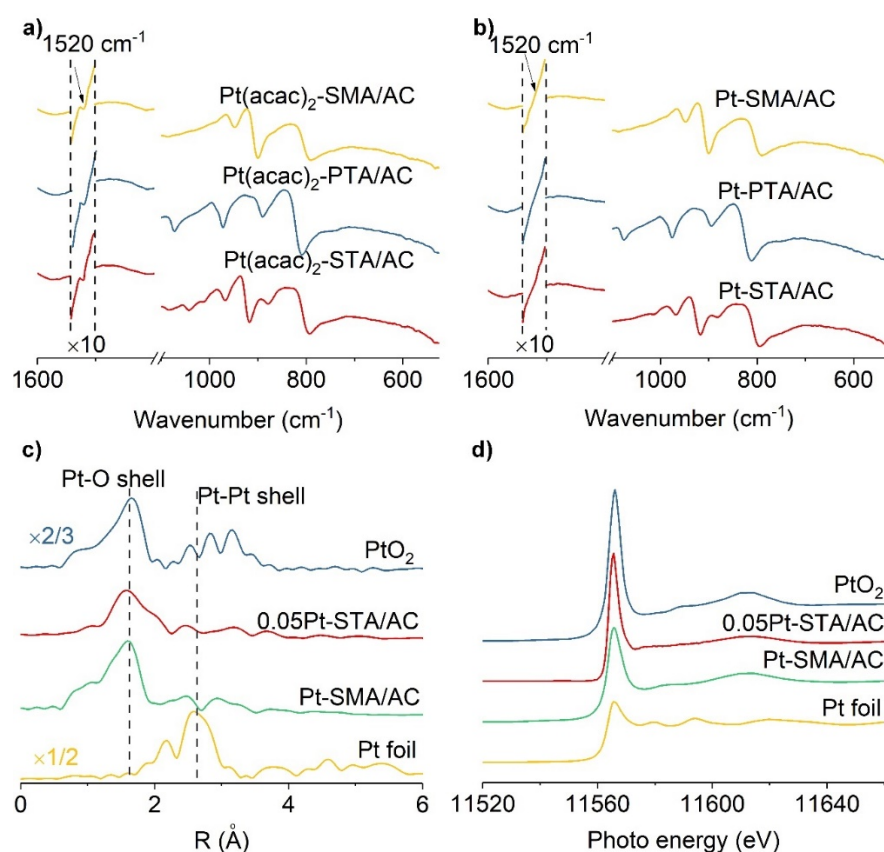
Figure 1. ATR-IR spectra (a, b) of Pt(acac)$_2$-polyoxometalate/AC with different polyoxometalates before and after reduction in 5 % H_2 balanced in N_2 at 170 °C for 1 h. The peak located at 1520 cm^{-1} is assigned to the C=O vibration of acac^{-1}; c) Fourier transform EXAFS spectra at Pt L$_3$ for Pt foil, Pt-SMA/AC, 0.05Pt-STA/AC and PtO$_2$. Δk = 3–13 Å^{-1}; d) Pt L$_3$ edge XANES spectra of Pt foil, Pt-SMA/AC, 0.05Pt-STA/AC and PtO$_2$, with the white-line intensities following a decreasing trend: PtO$_2$ (3.68) > Pt-SMA/AC (1.83) > Pt foil (1.20). The values included in the parenthesis correspond to the absorption height after normalization.
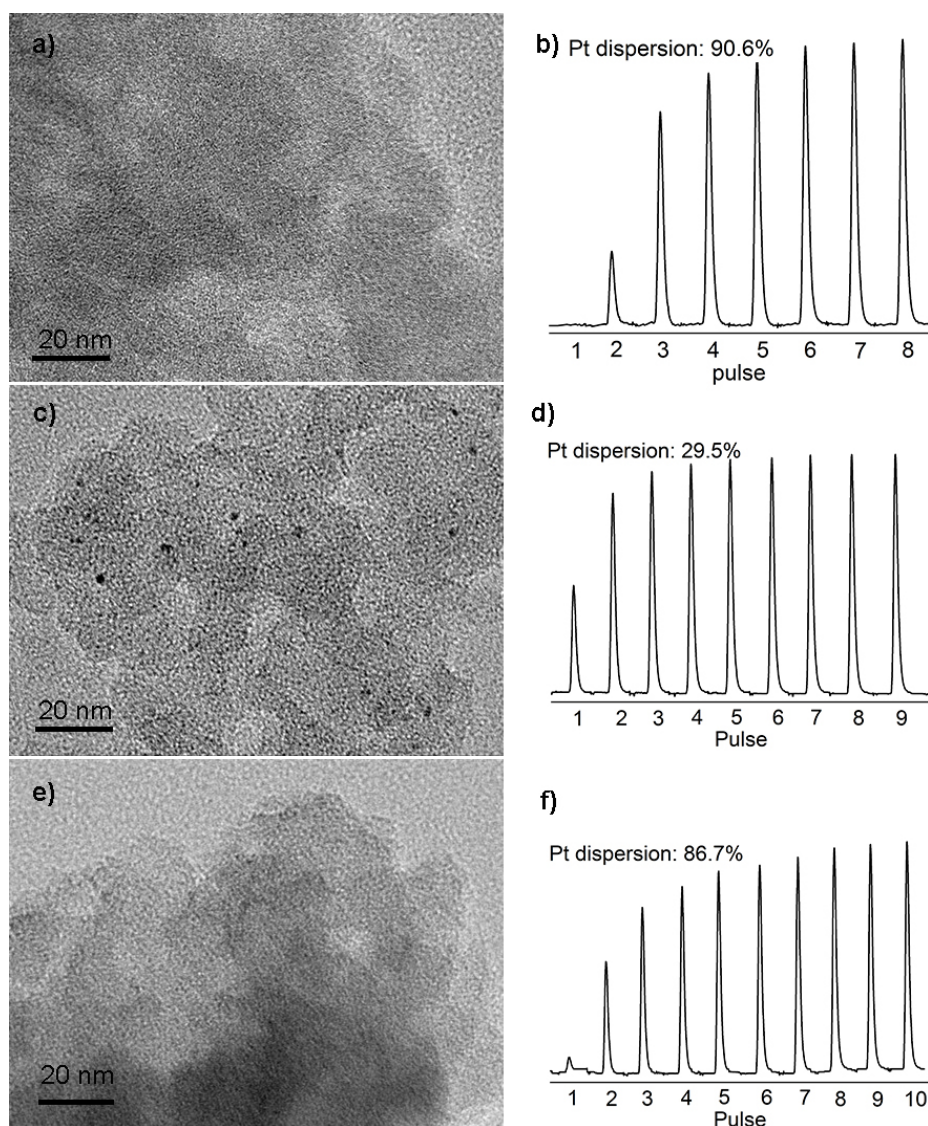
Figure 2. TEM images for a) Pt-SMA/AC, c) Pt-PTA/AC and e) Pt-STA/AC. EDX analyses based on the above images exhibited that the Pt and polyoxometalates are dispersed well on AC with the Pt loadings close to 0.9 wt%. H_2 pulse titration profiles of b) Pt-SMA/AC, d) Pt-PTA/AC and f) Pt-STA/AC. The titration ends as the peak intensities reach constant. For a titration, after pretreatment in air at 100 °C for 30 min, 100 mL/min of N_2 is used as the carrier gas at 100 °C and 159 μL/pulse of H_2 is employed for titrating 150 mg of catalyst.

To further prove whether atomically dispersed Pt species were obtained, extended X-ray absorption fine structure spectroscopy (EXAFS) was employed to identify the coordination environment of Pt species on different polyoxometalates. Pt–Pt shell located at ~2.7 Å was not

8

detected in the EXAFS at Pt L_3 edge of Pt-SMA/AC and Pt-STA/AC (Figure 1c), convincingly manifesting that the majority of Pt species existed as isolated atoms without metal bonding in these two samples. The curve fitting parameters are provided in Table S4. As expected, the coordination numbers of Pt-Pt for both catalysts are negligible, which is a typical characteristic of Pt SACs. Besides, the Pt-O coordination numbers for both are close to 4, revealing that each Pt atom plausibly siting at the four-fold hollow site of polyoxometalates. As Pt L_3-edge (11.5 keV) is interfered with W L_2-edge (11.5 keV),[53] it is impossible to measure Pt L_3-edge XAS spectrum in the presence of W at such high loadings because of the presence of W L_2-edge. Instead, we used high-energy resolution fluorescence detection (HERFD) EXAFS technique to perform the analysis on diluted Pt-STA/AC. Therefore, the XAS spectra of 0.05Pt-STA/AC, which contains only 0.05 wt% of Pt were collected to prove that Pt SACs were achieved on STA, with similar Pt-O coordinating mode. The details will be reported separately but the analysis further hints at the single-atom identity of Pt in Pt-STA/AC. *Based on all the structural characterizations above, we conclude that Pt exists dominantly as single atoms in Pt-SMA/AC, Pt-PMA/AC and Pt-STA/AC, but as small NPs in Pt-PTA/AC*.

XANES were employed to study the charge interaction between single Pt atoms and polyoxometalates supports (Figure 1d). As depicted in Figure 4b, the white line intensities of Pt at 11568 eV[54] for Pt-PMA/AC and Pt-SMA/AC are similar, in between the intensity values of Pt foil and PtO_2, confirming that Pt atoms in Pt-SMA/AC were positively charged after reduction with H_2. The valence of Pt is estimated as 1.3 based on liner combination analysis suggesting charge transfer from Pt to polyoxometalate, consistent with the above-proposed Pt-O coordination mode. For Pt-PTA/AC and Pt-STA/AC, XPS technique was utilized to analyse the charge state of Pt. In the deconvoluted XPS curve of Pt 4f electron in Pt-PTA/AC (Figure S11), around 3/4 of the total Pt atoms are reduced to Pt^0 with a binding energy of 71.0 eV[55] and only 1/4 of Pt atoms are positively charged which may exist at the interface between Pt clusters

9

and oxides. On the other hand, all the Pt species are positively charged in Pt-STA/AC, suggesting a much stronger electronic interaction between Pt atoms and O species. XPS analysis is also in full agreements with the proposed structure of the catalysts where Pt stays in the form of NPs in Pt-PTA/AC and in single-atom state in Pt-STA/AC. XPS spectra of Mo and W were also recorded (Figure S12 and S13), which showed no reduction of polyoxometalates. Another evidence demonstrating the interaction between Pt and polyoxometalate is change of acidity after Pt incorporation. It has been reported that the acidity usually follows the order: PMA>STA>SMA.[56] However, the acidity determined by NH$_3$-TPD after Pt deposition (Figure S14) follows, based on desorption temperature, a different order: Pt-STA/AC (328 °C) $\approx$ Pt-SMA/AC (326 °C)> Pt-PMA/AC (270 °C). TEM and ATR-IR were employed to examine the thermal stability of Pt SACs, as shown in Figure S15 and Figure S16. As the the Keggin structure of polyoxometalates broke down at 300 °C, Pt single atoms formed aggregates without strong stabilization effect.

To gain a deeper understanding of Pt coordination on polyoxometalate deposited AC, density function theoretical (DFT) calculations were performed to study the most stable adsorption sites of Pt atoms in three systems (Pt-SMA/AC, Pt-PTA/AC and Pt-STA/AC) where AC has been modelled by a 2D graphene layer. For comparison, the result of Pt-PMA/AC which has been reported in our previous study is also listed.[45] Four different surface sites (four-fold hollow site (4-H, Figure 3a), three-fold hollow site surrounded by three O$_{br}$ atoms (3-H_O$_{br}$), the three-fold hollow site formed by one O$_c$ atom and two O$_{br}$ atoms (3-H_O$_c$), together with the O$_c$-O$_{br}$ bridge sites (Figure 3b,c) were investigated for the adsorption behaviors of Pt atoms on the polyoxometalates. The average bond lengths for the most important bonds in graphene supported polyoxometalates, the adsorption energies of Pt atoms and the Pt-O bond lengths are summarized in Table 1 and Table S5.
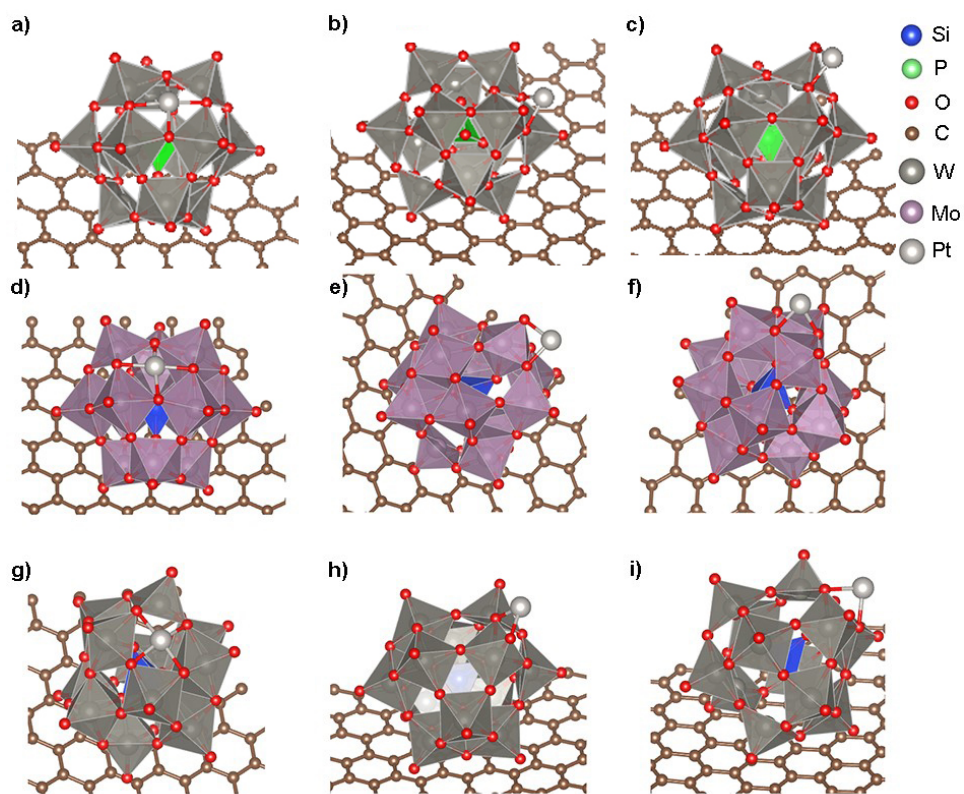
Figure 3. Optimized structures of Pt-polyoxometalate/Graphene systems: a-c shows that Pt adsorbed on PTA/Graphene and specifically a) 4-H site, b) O_c-O_{br} bridge site, c) O_{br}-O_{br} bridge site; d-f shows Pt adsorption on SMA/graphene system and specifically d) 4-H site, e) O_c-O_{br} bridge site, f) O_{br}-O_{br} bridge site; g-i shows Pt adsorption on STA/graphene system and specifically g) 4-H site, h) O_c-O_{br} bridge site, i) O_{br}-O_{br} bridge site; Pt adsorption on PMA system were reported in our previous paper.[45]

Table 1. Adsorption energies and important geometry parameters for Pt-[polyoxometalate]/Graphene adsorption systems.

[polyoxometalate]	Adsorption site	Coordination number of Pt	E_{ad} (eV)[a]	Pt-O bond length (Å)	Bader charge (Magnetization)
PMA[45]	4-H	4	-5.72	2.00, 2.01, 2.01, 2.02	1.02 (1.0)
	O_{br}-O_{br} bridge site	2	-3.94	1.95, 1.95	
	O_c-O_{br} bridge site	2	-3.56	1.94, 1.95	
PTA	4-H	4	-4.96	2.02, 2.02, 2.03, 2.03	
	O_{br}-O_{br} bridge site	2	-3.12	2.00, 2.00	1.04(1.0)
	O_c-O_{br} bridge site	2	-3.24	2.00, 1.97	
STA	4-H	4	-6.17	1.98, 1.98, 2.04, 2.04	
	O_{br}-O_{br} bridge site	2	-4.47	1.96, 1.96	1.28(0.0)
	O_c-O_{br} bridge site	2	-4.32	1.95, 1.92	
SMA	4-H	4	-6.91	1.95, 1.96, 2.03, 2.03	
	O_{br}-O_{br} bridge site	2	-4.96	1.95, 1.95	1.27(0.0)
	O_c-O_{br} bridge site	2	-4.62	1.90, 1.93	

[a]$E_{ad} = E_{Pt+[polyoxometalate]\text{-}G} - E_{[polyoxometalate]\text{-}G} - E_{Pt}$. $E_{Pt+[KA]\text{-}G}$ refers to the total energy of the Pt adsorbed [polyoxometalate] on carbon system, $E_{[polyoxometalate]\text{-}G}$ is the energy of supported [polyoxometalate] cluster and E_{Pt} means the energy for a Pt atom. In this article, negative values correspond to exothermic adsorption.

As shown in Table 1, among different possible adsorption sites, one Pt atom clearly prefers

to be coordinated with four oxygen atoms (4-H site) which matches well with the knowledge

in classic coordination chemistry that Pt prefers to coordinate with four ligands.[57-58] When Pt is initially placed at the 3-H site, the atom will move upon energy optimization to an O_{br}-O_{br} or O_c-O_{br} bridge site. On the preferred 4-H site, one Pt atom and 4 surrounding O atoms adopt a "quasi-square-planar" geometry with only small variations in Pt-O bond lengths. The calculated results illustrated that the average Pt-O bond lengths of Pt-polyoxometalate/AC followed the sequence: Pt-SMA/AC (1.99 Å) < Pt-STA (2.01 Å) = Pt-PMA/AC (2.01 Å) < Pt-PTA/AC (2.025 Å). The different bond lengths also suggest different interactions between Pt and O in Pt-polyoxometalate, Pt-PTA/AC having the longest average Pt-O bond length. The Bader charges and the total magnetization density (mostly located at Pt site) are also shown in Table 1. The results indicate that Pt cations show 3+ valence state on PMA and PTA, while slightly higher oxidation state (4+) on SMA and STA (see Figure S21). The absolute values of adsorption energies of Pt on 4-H site, which suggests the strengths of Pt binding to polyoxometalates, follow the order of Pt-SMA (6.91 eV) > Pt-STA (6.17 eV) > Pt-PMA/AC (5.72 eV) > Pt-PTA/AC (4.96 eV) and the results are consistent with the bader charge analysis (Table 1), which shows that on SMA and STA, there is a rather large charge transfer from Pt atoms to the supports. The DFT calculated cohesive energy of bulk Pt is 5.50 eV with the PBE functional (compared with experimental result of 5.85 eV),[59] which lays between the absolute values of Pt-PMA/AC and Pt-PTA/AC. *Comparison between the cohesive energy of Pt bulk and adsorption energy of polyoxometalate supported Pt clearly provides a predictive view for the formation of Pt NPs in Pt-PTA/AC and Pt SACs in the other three systems*: Pt atoms can stay atomically dispersed if the interaction between Pt and supports is stronger than the cohesive energy of bulk Pt atoms (PBE predicted cohesive energy is used here for consistency), while they will agglomerate if the binding energy falls below that. We summarized DFT adsorption energies of Pt single-atoms on various supports reported in the literature in Table S6. In almost all cases, the binding energy between Pt and the support is larger than 5.50 eV.

Clearly and simply, the absolute value of the Pt atom adsorption energy on the oxide support should be able to overcome the cohesive energy of bulk Pt to obtain stable Pt SACs. This very simple parameter (Pt cohesive energy) provides an important tool for predicting whether Pt SACs could be successfully obtained in catalyst design and such an approach might be extended to predict the preparation of SACs based on other metals.

**Catalytic performance of Pt-polyoxometalates/AC**

How does metal-support interaction influence catalysis is a central question. Support-metal interaction is indeed a key factor that differentiates the catalytic performance of different polyoxometalates.[18, 30, 60] Comparative study on the catalytic performance of the catalysts is key to unveil the relationship between stability and reactivity over Pt SACs.

As mentioned above, propene hydrogenation over SACs is sensitive to the support. Meanwhile, many industrial reactions (e.g. hydroformylation reaction) require the co-feed of catalyst with alkene and/or H_2. Thus, hydrogenation of propene was first used to probe the catalytic performance of different Pt SACs. The turnover frequency (TOF) values were determined at varying temperatures while the conversion was controlled below 10%. All three Pt SACs are active for the reaction with TOF values ranging from 100-180 h^{-1} at 30 °C and increased to 150-350 h^{-1} at 50 °C. In general, the influence of stabilizing effect from supports for metal species on the catalytic performance is complex. The metal-support interaction must be strong enough to suppress the aggregation. However, very strong interaction may also end up with inert catalytic centers for reactions following Langmuir–Hinshelwood mechanism.[61] As described in Figure 4a,b, the reaction rates over Pt-SMA/AC and Pt-STA/AC are similar, while the rate of Pt-PMA/AC is ca. 1.5 times faster. The activation energies for each catalyst determined in the range of 30 to 50 °C are 24.9 kJ/mol for Pt-PMA/AC, 26.3 kJ/mol for Pt-SMA/AC, and 25.8 kJ/mol for Pt-STA/AC. These activation energies are almost identical,

regardless of the Pt adsorption energy, suggesting that the stabilizing effect of polyoxometalates does not affect the reactivity. We also performed hydrogenation reactions of 1,3-butadiene (mixed with propene) and phenylacetylene to reflect catalytic properties in hydrogenation of diene and alkyne, as shown in Figure 5, Figure S17, S18 and Table S7, S8. The Pt SACs have tendency to promote the selective transformation of 1,3-butadine to butene when the temperature is below 100 °C, which is consistent to previous reports on metal SACs.[37, 39] The activity of the three Pt_1 catalysts in 1,3-butadine hydrogenation is similar throughout the tested temperature range (25-100 °C). Conversion of propene was also observed, in particular under higher temperatures, but again the TOF are almost the same with the three catalysts (reflected in Figure 5b). Such phenomenon was further observed in phenylacetylene hydrogenation (Table S7). *These catalytic results manifest that different polyoxometalates supported Pt SACs may follow a similar reaction pathway and activation barrier in hydrogenation reactions.* The theoretical insights of this are provided in a later part.
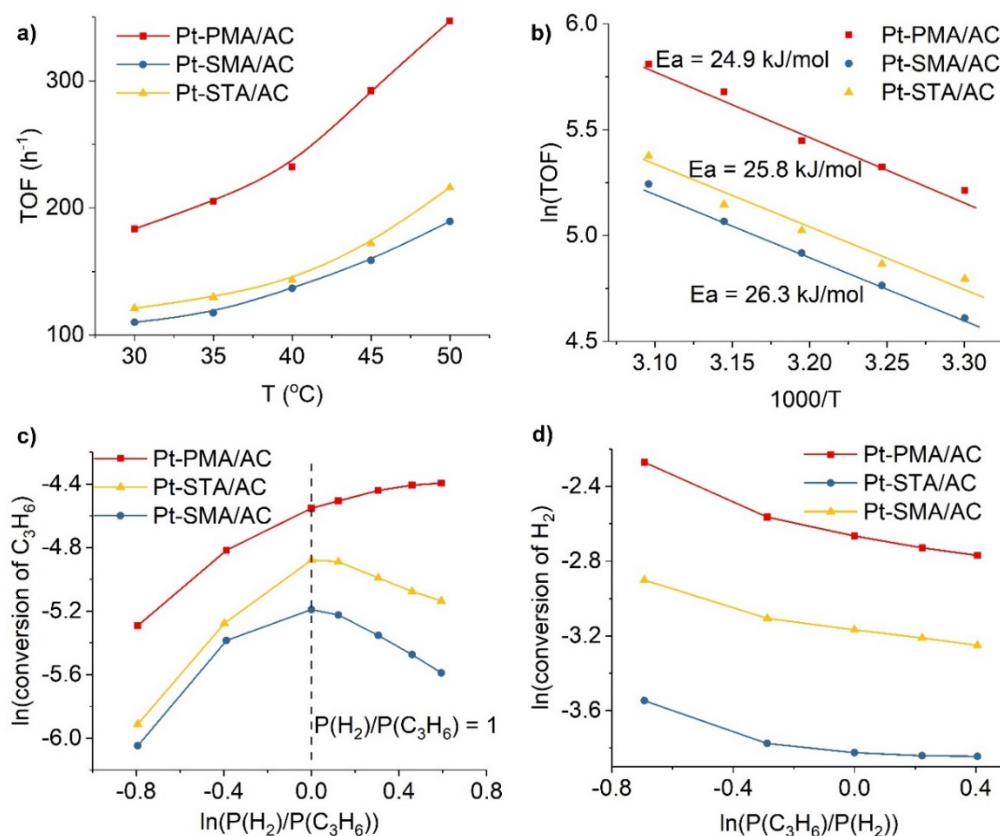
Figure 4. a) TOF values and Arrhenius plots (b) of propene hydrogenation rates over different isolated Pt-polyoxometalate/AC catalysts. Reaction rates were measured in 3.3% propene, 3.3% H_2 balanced in Helium, the total flow rate was 80 mL min^{-1}. TOF values were calculated with the Pt dispersion results from H_2-O_2 titration experiment. Propene hydrogenation rates over different Pt-polyoxometalate/AC catalysts as a function of H_2 partial pressure (c) and a function of propene partial pressure (d). The rates were measured at 50 °C over 5 mg of each catalyst, GHSV = 48000 h^{-1}.
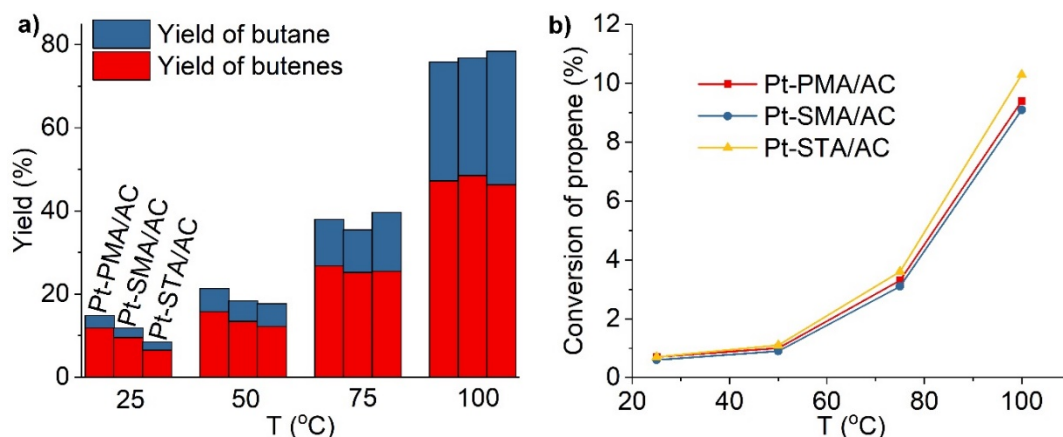
Figure 5. Catalytic hydrogenation performance of 1,3-butadiene. Reaction conditions: mixed gas (2% of 1,3-butadiene, 20% of propene, 16% of H_2, 62% of He); flow rate: 40 ml/min; ambient pressure; 6.3 mg of a certain catalyst mixed with 13.7 mg AC before using.

For propene hydrogenation, the dependency of reaction rates on the partial pressures of H_2 and propene were investigated (Figure 4c, d). Figure 4d shows that the conversion decreases as the partial pressure of propene increases but in which, the reaction order is almost zero. This suggests propene strongly adsorbs on the catalyst, which is consistent with the calculated stronger propene adsorption in Table 2. Therefore, we can expect that reaction starts from propene adsorption first and then it reacts with subsequent adsorbed H_2. On the other hand, reaction kinetics is more sensitive to the H_2 partial pressure. As shown in Figure 4(c), increasing partial pressure of H_2 would monotonously increase the conversion (in the studied range) on Pt-PMA/AC, but decreases the conversion on Pt-SMA/AC and Pt-STA/AC at higher H_2 partial pressure. As we will demonstrate in the reaction mechanism studies (following section), the reactions take place starting from propene adsorption and react with subsequent H_2. Therefore, if propene adsorption slows down, the overall reaction rate will also be compromised.

We can explain the different reaction orders of H_2 in Figure 4(c) with kinetic effects. Because Pt-SMA and Pt-STA show larger H_2 absorption energy than Pt-PMA (Table 2), they could be partially covered by H_2 with increasing H_2 pressure. As shown in Table S15, increasing the H_2

partial pressure or increasing the adsorption energy of H_2 (even by a small amount) will end up with that adsorption equilibrium preferring the absorption side. Table 2 also shows that Pt-SMA and Pt-STA prefer co-adsorption of two H_2 molecules, the differential adsorption energy of the second H_2 being stronger. We can expect that a significant amount of the Pt-SMA and Pt-STA catalyst would be occupied by two H_2 at higher pressure. Then the propene adsorption would require the removal of one H_2, which is still possible in thermodynamically but less favorable than in the low H_2 pressure case (Table 2). This explains the decrease of the reaction rate for Pt-SMA and Pt-STA at high $P(H_2)/P(C_3H_6)$ in Figure 4(c). Pt-PMA follows a quite different scenario. It hardly adsorbs H_2 without the help of propene, therefore we can expect that in a reasonable range of H_2 partial pressure, the Pt site on Pt-PMA is always empty for propene adsorption. Therefore, increasing H_2 partial pressure would not impact conversion as in indicated in Figure 4(c).

Table 2. Adsorption energy of propene, H_2 on Pt SACs. The adsorption energy is defined as $E_{ads} = E_{molecule+PtSAC} - E_{molecule} - E_{PtSAC}$.

E_{ads}	Pt-PMA/AC	Pt-SMA/AC	Pt-STA/AC
E_{ads} (H_2)/ eV	-0.22	-0.50	-0.64
E_{ads} (propene)/eV	-1.17	-1.59	-1.79
E_{ads} (H_2+propene)/eV	-1.78	-2.14	-2.54
ΔE_{ads}, synergetic effect /eV[a]	-0.39	-0.05	-0.11
E_{ads} (H_2+H_2)/eV[b]	-0.37(-0.16)	-1.10(-0.60)	-1.36(-0.71)
ΔE[c]	-1.40	-1.04	-1.12

a. The synergetic effect is defined as $E_{ads}(H_2+propene) - E_{ads}(H_2) - E_{ads}(propene)$

b. Number in parenthesis is the differential adsorption energy of second H_2

c. $\Delta E = E_{ads}(propene+H_2) + E^{gas}(H_2) - E_{ads}(H_2+H_2) + E^{gas}(propene)$

Simulated reaction pathways

We further investigated the reaction pathways for H_2 adsorption, dissociation and its diffusion on the bare Pt-PMA/AC. Results are shown in Figure 6a. Firstly, H_2 adsorbs on the Pt atom as an activated non-dissociated H_2 molecule with a low adsorption energy (-0.12 eV in Figure 6a) then adsorbed H_2 dissociates through a very small barrier (about 0.13 eV). The best configuration has an adsorption energy (-0.22 eV) is much smaller compared with that on Pt(111) (-1.04 eV per H_2)[62] which means that H_2 adsorption is rather difficult on those single Pt catalysts. After dissociation, the possible pathways for one H atom to spill over to a nearby oxygen atom from the support are also located. Results show that the migration requires a large barrier (almost 1 eV) and the energy of the transition state is even 0.78 eV higher than the energy of gas phase H_2. Therefore, H is not expected to be able to efficiently migrate to oxygen atoms on the support at low reaction temperatures, although the second spill over is an exothermic process.
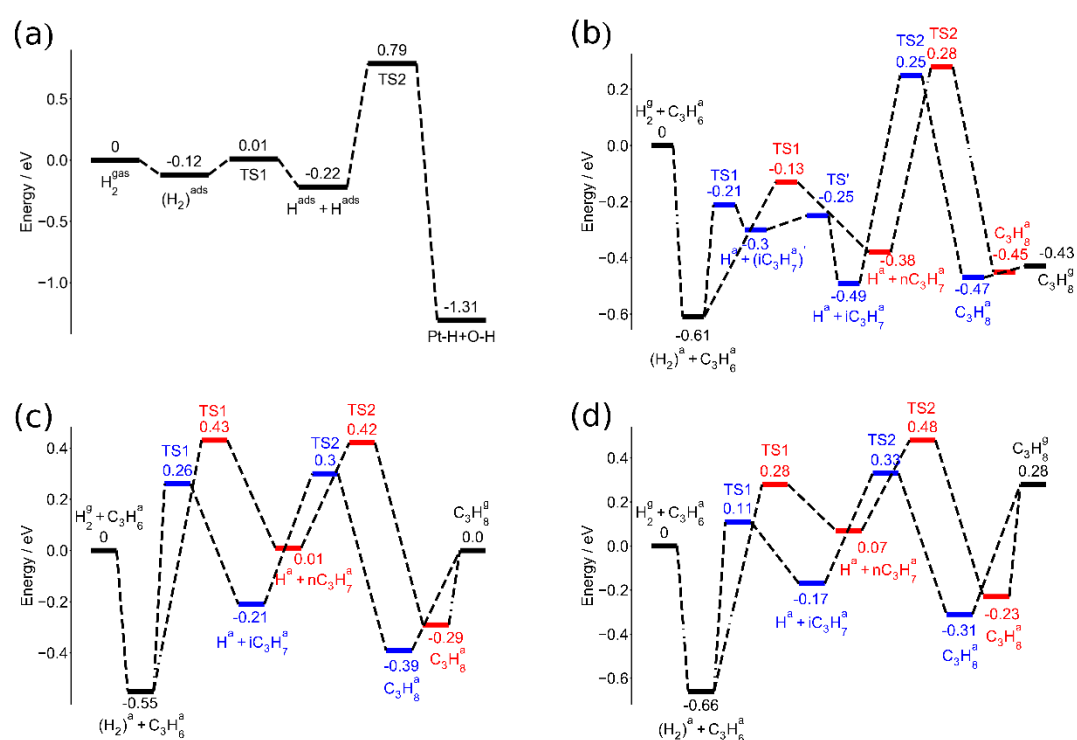
Figure 6. a) H_2 dissociation and spillover on PMA support Pt catalyst. Gas phase H_2 is used as energy reference. b-d) calculated reaction profiles for propene hydrogenation on three different polyoxometalate supported Pt SACs: b) Pt-PMA/AC; c) Pt-SMA/AC; d) Pt-STA/AC. Each

reaction profile starts from H_2 (gas) plus adsorbed propene as zero reference. The blue color illustrates the *iso*-propyl channel and the red color illustrates the *n*-propyl channel. Superscript *g* stands for gas phase species and superscript *a* stands for adsorbed species. $i - C_3H_7^a$ stands for adsorbed isopropyl group. $(i - C_3H_7^a)'$ (on Pt-PMA) stands for a metastable structure of an intermediate, which undergoes a small barrier to the more stable $i - C_3H_7^a$. All the energies are in eV. The key structures of intermediates and transition state structures are shown in Table S7-S10.

Then we studied the reaction pathways of propene hydrogenation on three different model SACs. For every SAC catalyst, propene hydrogenation has two main reaction channels according to the intermediate after the first hydrogenation step. They are labelled as *iso*-propyl channel (adsorbed *iso*-propyl is the intermediate after the first hydrogenation step) and *n*-propyl channel. Starting from the adsorbed propene on Pt-polyoxometalate catalyst, gas phase H_2 adsorption as well as subsequent pathways of propene hydrogenation reaction are optimized and the calculated energy profiles for both channels are shown in Figure 6b-d. It shows that the reactions take place with a similar mechanism: two successive hydrogenation steps produce the intermediate and the final product. The *iso*-propyl channel on Pt-PMA is slightly different, the first hydrogenation product is a metastable structure (but possess the identity of *iso*-propyl) and further reconstructs to a more stable structure with a small barrier.
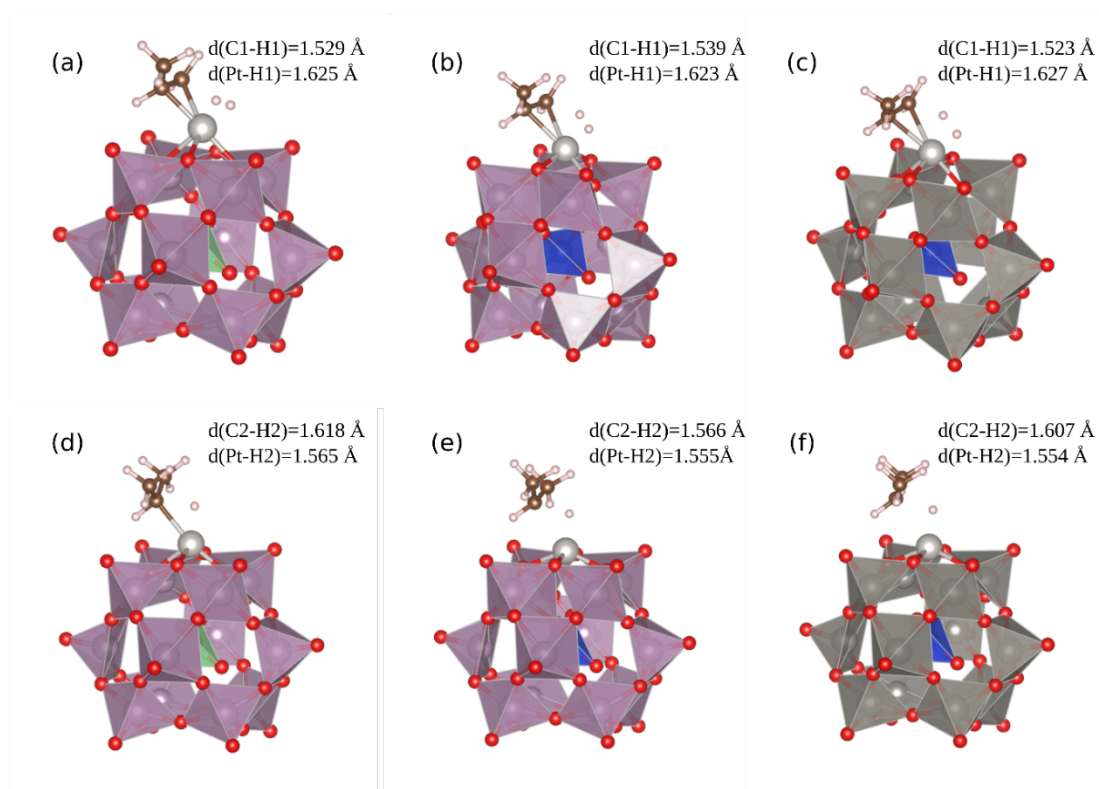
Figure 6(b-d) shows that *iso*-propyl channels are generally more competitive than the *n*-propyl channel (blue profiles), where both the transition state structures and the reaction intermediates along the *iso*-propyl channel exhibit lower energies than those along *n*-propyl channels. Considering that methyl is an electron donating group, secondary carbons in the *iso*-propyl group are more favorable to bond with cationic Pt atoms and therefore *iso*-propyl channels are more energetically competitive. Figure 7 shows the structures of TS1s and TS2s along the *iso*-propyl channels as well as some important bond lengths. Other calculated local

minima and transition state structures are listed in Supporting Materials Table S9 (for Pt-PMA/AC), Table S10 (for Pt-SMA/AC) and Table S11 (for Pt-STA/AC). The barrier to form the *iso*-propyl is markedly smaller, on Pt-PMA/AC (0.40 eV) compared to the other two catalysts (~0.8 eV). This is associated with a more stable iso-propyl intermediate on Pt-PMA/AC. The second hydrogen step forming propane follow a standard "reductive elimination" mechanism with this time a higher barrier for Pt-PMA/AC (0.73 eV) compared to the other two catalysts (~0.5 eV).

In general, the reaction takes place in a very similar way among the three Pt-SACs: all the steps only involve the Pt_1 species while polyoxometalate acts as anchoring site during the reaction. This is distinct from the alkene hydrogenation pathways on extended surfaces.[63] The adsorbed propene appears as one π-bonded species (see Table S9–S11) because there is only one Pt atom present. This should not be detrimental to the reactivity because of the di-σ-bonding species has proven to be irrelevant for the hydrogenation of ethylene.[64] The second common feature is that the TS of second hydrogenation step is always higher in energy for all the *iso*-propyl channels, and therefore, it is the rate-determining steps for the overall kinetics and thus determines the observed reaction barriers. The final product (propane) is weakly adsorbed on Pt-PMA, but rather strongly adsorbed on Pt-STA and Pt-SMA, which results from the more cationic nature of Pt on Pt-SMA and Pt-STA. The cationic Pt can polarize the C-H bond and induce a stronger adsorption.

One interesting point is that H_2 preferentially adsorb as a molecular entity on the propene pre-covered Pt (with a bond length of about 0.8~0.9 Å). H_2 does not dissociate, but the hydrogenation takes place directly from the adsorbed H_2 precursor, one H atom being shifted to one C atom. We carefully proved this by calculating the IRC from the transition state structures. The C-H bond distance was slightly elongated along the imaginary mode (by 0.03, 0.05 and 0.08 Å respectively) from the transition state structures (TS1), then structures are

optimized by a steepest descent algorithm with a very small step (POTIM=0.02 in VASP) and the velocities are projected out at every ionic steps. Essentially, the trajectory mimics the intrinsic reaction coordinate (IRC) of the first hydrogenation step. The results show that the first hydrogenation reaction step indeed takes place directly from the molecular adsorbed H_2 rather than the dissociated H atoms. Hydrogenation experiments using 1:1 D_2/H_2 mixture were next performed over the Pt SACs. All three Pt SACs provided scrambling products (Figure S19 and Table S13, S14). In the case of propene hydrogenation over the Pt-STA/AC catalyst, for instance, ca. 50% product contains 2 newly added H atoms, 25% product contains 2 newly added D atoms, and 25% product contains 1D and 1H atoms. Such phenomena suggest that the SACs promoted H_2-D_2 exchange in situ. In a subsequently designed controlled experiment, 1:1 H_2/D_2 mixture was passed through the catalyst at room temperature with the same space velocity as used for propene hydrogenation. HD gas accounts as much as 43% in the product stream (Figure S20).

(a) d(C1-H1)=1.529 Å d(Pt-H1)=1.625 Å
(b) d(C1-H1)=1.539 Å d(Pt-H1)=1.623 Å
(c) d(C1-H1)=1.523 Å d(Pt-H1)=1.627 Å
(d) d(C2-H2)=1.618 Å d(Pt-H2)=1.565 Å
(e) d(C2-H2)=1.566 Å d(Pt-H2)=1.555Å
(f) d(C2-H2)=1.607 Å d(Pt-H2)=1.554 Å

Figure 7. The transition state structures in *iso*-propyl channel and different catalyst (a) TS1 on

Pt-PMA, (b)TS1 on Pt-SMA, (c) TS1 on Pt-STA, (d) TS2 on Pt-PMA, (e) TS2 on Pt-SMA, (f) TS2 on Pt-SMA. The important bond lengths are shown. The C1 is the terminal carbon atom in the olefin bond and C2 is the middle carbon atom in the olefin bond. H1 and H2 are hydrogen atoms forming C1-H1 bond and C2-H2 bond respectively.

The reason to use propene adsorbed structure as starting point is that Pt atoms are expected to be pre-occupied by strongly adsorbed propene (shown in Table 2) and then the reactivity will be determined by the accessibility of the subsequent H_2 to the "empty site", i.e. one propene pre-adsorbed Pt sites. Experimental results also show that the reaction order of propene is nearly zero (small negative value in Figure 4(d)), which also supports this assumption. It should be noted that H_2 adsorption energy on those Pt-SACs are much smaller than that on Pt(111) surface or defective Pt clusters (-1.04 eV per H_2 on Pt(111) by PBE functional and even stronger on Pt(100) and clusters.[62, 67] The Gibbs free energy change of H_2 adsorption on those Pt catalysts and the equilibrium temperature (T_c) between adsorbed H_2 and gas phase H_2 have been calculated using experimental conditions (Table S15). It is found that the experimental temperature is high enough to prevent significant adsorption of H_2 on the propene pre-occupied the Pt sites. In this case, the experimental measured apparent activation barriers corresponds to the sum of total barrier and reactant adsorption enthalpy (Supporting Information equations S1-S8). Effectively the apparent reaction barriers are reduced because the reaction adsorption enthalpy is negative. [65-66] Combining this method and data from Figure 6, the simulated apparent reaction barriers for Pt-PMA/AC, Pt-SMA/AC and Pt-STA/AC are 0.25 eV (24.1 kJ/mol), 0.30 eV (28.0 kJ/mol) and 0.33 eV (31.8 kJ/mol) respectively, where the iso-propyl channel is responsible for the observed activities. The results agree very well with the experimental measured values.

Although hydrogen spillover is not easy on Pt-SACs because of the high barrier shown in Figure 6(a), there is also a small that chance heterolytically activated H_2 exist in this system.

Therefore, we also considered a partial reduced model in which the catalytic model starts from the final product of Figure 6(a), but the partial reduce model does not efficiently complete the hydrogenation reactions. The details are explained in the Figure S22 and Table S16.

Conclusion

The stabilization effect of oxide supports for noble metal atoms are essential for designing SACs, as too weak interaction results in atom aggregation into NPs. In this work, a combination of experimental results and DFT analyses over a series of polyoxometalate stabilized Pt SACs shows that the nature of the core main group element (P, Si) and of the transition metal (Mo, W) can modulate the Pt binding energy by ~2 eV (40 %). Stable Pt SACs are simply obtained when the adsorption energy of Pt on the support is higher than the cohesive energy of Pt. Following similar geometric structures and coordination environment of the Pt SACs, their reactivity in propene hydrogenation were systematically investigated using both experimental and theoretical approaches to establish the structure-activity relationships. Both hydrogen and propene are activated on the Pt single-atom, while the neighboring oxygen atoms on the support do not directly participate in catalysis. In general, H_2 adsorbs much weaker on the Pt SACs than on a metallic Pt (111) surface because of the large charge transfer between the support and Pt atom.[62] Propene and H_2 and coadsorbed on the cationic Pt in a molecular form and one H from the H_2 unit is transferred to propene, preferentially forming isopropyl, while the migration of the remaining H atom forms propane. The cationic Pt atoms show rather large intrinsic energy barriers but small apparent activation energies (~25 kJ.mol^{-1}) since H_2 adsorption is endergonic in reaction conditions and the adsorption equilibrium constant is small. On the other hand, despite the large difference in Pt-support binding energy, the measured activation energies over three Pt SACs are essentially the same. This matches well with the DFT reaction pathway calculations and shows that high stability and high activity are not contradictory for

single atom catalysts.

This paper provides some clues for SAC design in the future. First, the minimum adsorption energy of a metal atom on the support to make stable SACs seems to be equivalent to the cohesive energy of that bulk metal, offering a predictive view how to identify the right combination of metal and support to synthesize SACs. Second, enhancing the stability of SACs does not necessarily decrease the activity of the catalysts, since the total effective barriers are results of several competing factors. Although strong metal-support interaction is detrimental to the adsorption of reactant on metal center in general, but it induces more available sites and essentially decreased the effective barrier in the overall kinetics. Generally, it is contradictory to obtain stable SACs and to pursue low energy barriers for interested reactions because the strong metal-support interaction would induce an inert catalytic center. While, our studies show it is feasible to obtain an optimal support, which provides strong metal-support interaction to resist catalyst aggregation together with fast reaction kinetics.

Materials, Experiment and Computational Procedures

Materials

Phosphomolybdic acid hydrates (PMA, ACS reagent), phosphotungstic acid hydrate (PTA, reagent grade), silicomolybdic acid solution ($H_4SiMo_{12}O_{40}$, SMA) and tungstosilicic acid ($H_4SiW_{12}O_{40}$, STA), platinum (II) acetylacetonate (Pt(acac)$_2$, 97%) were from Sigma Aldrich. Acetone (AR) was purchased from Fisher Scientific. Hydrochloric acid (37%) and nitric acid (65%), ethyl acetate (AR) were provided from Merk Pte. Ltd. Activated carbon (AC) was supplied by Sinopharm Chemical Reagent (SCR). All the chemicals above were simply used as received.

Catalyst Preparation

Preparation of Pt-polyoxometalate/AC. Taking Pt-SMA/AC as an example, in a 15 mL centrifuge tube containing 0.9 g AC, a SMA solution (54 μmol, 100 mg in 10 mL acetone) was introduced dropwise and mixed with AC by vigorous stirring (800 rpm for 5 h) and sonication (5 min). Afterwards, the sample was centrifuged at 8000 rpm for 3 min, and dried in an oven at 70 °C for 0.5 h. The same steps were applied for the loading of equimolar amount of Pt(acac)$_2$ (54 μmol, 0.017 g in 1 mL acetone) onto SMA modified AC. Finally, the dried sample was reduced in 5 % H$_2$/N$_2$ (gas flow rate: 100 mL/min) at 160 °C for 1 h.

For other Pt-polyoxometalate/AC, the molar amount of HPAs were kept the same. Only the amount of AC was adjusted to maintain the same total weight of catalysts. For comparison, catalyst without HPAs was also prepared using similar method at 0.5 wt% and 0.9 wt% loading. The solvent was vaporized after impregnation to ensure all Pt precursors are loaded on AC. The prepared catalysts were denoted as 0.5Pt/AC or 0.9Pt/AC.

Catalyst Characterization

For the structure characterization of Pt SACs, a series of techniques were employed: inductively coupled plasma optical emission spectrometry (ICP-OES), thermogravimetric analysis (TGA), N$_2$ adsorption with BET analysis, H$_2$-based temperature programmed reduction (TPR), temperature programmed desorption (TPD), H$_2$-O$_2$ adsorption and titration, transmission electron microscopy (TEM), X-ray diffraction (XRD) analysis, X-ray photoelectron spectra (XPS) attenuated total reflectance infrared (ATR-IR) spectroscopy analysis and X-ray absorption spectra (XAS) at Pt L$_3$-edge. The procedures are similar to previously literatures[45, 46] and are detailed in the supporting information.

Catalytic Performance Test

Hydrogenation of Propene

Reactivity studies for the hydrogenation of propene were performed in a 1 cm ID fixed bed

stainless flow reactor in a down flow configuration. 5 mg of the as-synthesized catalyst was added in the reactor. Before running the reactions, each catalyst was pre-treated with pure N_2 at for 0.5 h at 100 °C just to remove the absorbed water and air. Afterwards, a gas mixture of 3.3% (v/v) propene, 3.3% (v/v) H_2 and 93.4% (v/v) He (total flow of 80 ml min^{-1}) was introduced to the catalyst within an ascending temperature range (30–80 °C) and 1 atmosphere total pressure. GC-FID analysis was done every 5 °C after stabilization at that point for 0.5 h. After measuring the results at 80 °C, the system was cooled down for repetition at the above-mentioned temperature range for two more times. The activation energy was determined using the average rate values based on the 3 repeating measurements.

For the reaction order measurement, the reaction was performed at 50 °C and 1 atmosphere with a flow rate of 80 ml min^{-1}. When measuring the reaction rate with hydrogen pressure, the partial pressure of propene was maintained constant at 1.89 kPa and the partial pressure of hydrogen gas was adjusted from 0.855 kPa to 3.42 kPa. When determining the reaction order with respect to propene partial pressure, the partial pressure of hydrogen gas was set as a constant value of 2.52 kPa and the partial pressure of propene gas was adjusted from 1.26 kPa to 3.78 kPa.

Hydrogenation of Phenylacetylene.

Taking one molar (Pt : substrate = 1:1000) as an example. The substrate (27.4 μL, 0.25 mmol), catalyst (5 mg, Pt : substrate = 1:1000), and ethyl acetate (2 mL) were placed in a batch reactor. The reaction underwent at room temperature under H_2 (1.0 MPa) for 1 h. Reaction products were separated through filtering using a PTFE syringe filter whose pore diameter is 2 μm). Then, the products were analyzed by GC-FID and GC-MS. For the ratio of 1:2000, 1:4000 and 1:8000, the amount of substrate was changed accordingly while maintaining the same amount of catalysts.

Hydrogenation of 1,3-butadiene

This reaction was performed in a 1 cm ID fixed bed stainless flow reactor in a down flow configuration. The as-prepared catalyst (6.3 mg) was mixed with AC (13.7 mg) and was then placed in the reactor. Before running the reactions, each catalyst was pre-treated with pure N_2 0.5 h at 100 °C just to remove the absorbed water and air. Afterwards, Afterwards, a gas mixture (2% of propene, 20% of H_2 and 78% of He, v/v) with a total flow of 40 ml min^{-1} at 1 bar pressure was introduced at ascending temperature (25–100 °C) and 1 atmosphere total pressure. GC-FID analysis was done every 25 °C after stabilization at that point for 0.5 h. After measuring the results at 100 °C, the system was cooled down for repetition at the above-mentioned temperature range for two more times.

H_2-D_2 exchange experiment

H−D exchange experiment was performed in the above-mentioned flow reactor with an online mass spectrometry (MS, Hiden Analytical QCA) to evaluate gas mixtures at room temperature. As a reference, 20 ml/min of H_2 and 20 ml/min of D_2 were firstly introduced to the blank reactor without catalysts. After the signal was stable, intensities for the m/z values equaling to 1, 2, 3, 4, 28 and 32 were recorded for H, D, H_2, HD, D_2, N_2 and O_2, respectively. After this, 100 mg of Pt-SMA/AC was loaded into the reactor and identical procedures were employed for collecting the mass spectrum.

H_2-D_2 co-hydrogenation experiment

1. Hydrogenation of Propene with H_2 and D_2

With 100 mg of catalyst placed in the flow reactor, a feed gas consisting of 17% H_2 and 17% D_2, 6% C_3H_6 and 60% Ar was introduced at room temperature. After the signal was stable, intensities for the m/z values equaling to 43, 44, 45 and 46 were recorded for C_3H_7, C_3H_8, C_3H_6D, C_3H_7D, and $C_3H_6D_2$, respectively.

2. Hydrogenation of Phenylacetylene with H_2 and D_2

The substrate (27.4 μL, 0.25 mmol), catalyst (12.6 mg, Pt : substrate = 1:500), and ethyl acetate

(2 mL) were placed in a batch reactor, which was charged with 5 bar H_2 + 5 bar D_2. After rigorously stirring for 20 min, the reaction products were separated through filtering using a PTFE syringe filter whose pore diameter is 0.2 μm). Then, the products were analyzed by GC-MS. For comparison, reactions in pure H_2 or D_2 were also performed on Pt-STA/AC under the same reaction conditions.

Computational Details

DFT calculations in this work were conducted following a reported protocol[45] to investigate the stable structure models and energy profiles of Pt on graphene supported polyoxometalates using the Vienna Ab initio Simulation package (VASP). The projector augmented wave (PAW) approach was utilized for modelling the interaction between electrons and ions.[68-69] PBE form of the general gradient approximation (GGA) was employed for checking the profiles of the exchange energies as well as correlation energies.[70] During the computation process, the cut off energy for the employed plane-wave was adjusted as 400 eV.

As to the lattice constant of the graphene layer, the experimental value of 2.46 Å [71] was applied in the calculation, and the C-C bonding length is set as 1.42 Å. To simulate polyoxometalate–Graphene system, an 8x8 graphene supercell with 128 carbon atoms was chosen. Periodic boundary conditions were employed along all directions with a vacuum region of 22 Å between graphene layers. Due to the large supercell, the interaction between the system and its image can be avoided. We fully optimized the isolated polyoxometalates-graphene system and the results show that the graphene layer is almost flat and far from polyoxometalates supported Pt SAC group (C-O distance is larger than 3.0 Angstrom), which indicates the interaction between graphene and polyoxometalates is weak. The bond lengths of some main bonds match well with literature values [72]. The adsorption mode of Keggin anion $[PW_{12}O_{40}]^{3-}$ on graphene layer was previously studied showing that the interaction through S_4 symmetrical axis is more favourable than that via C_3 axis [73]. Thus, the adsorption mode with S_4 axis of polyoxometalate

vertical to graphene layer was considered here. In this work, the adsorption energy of Pt atom adsorbed on polyoxometalate-Graphene is defined as $E_{ad} = E_{Pt+polyoxometalate-G} - E_{polyoxometalate-G} - E_{Pt}$, where the $E_{Pt+[PMO]-G}$ standard for the energy of the Pt adsorbed on graphene supported polyoxometalates, $E_{[PMoO]-G}$ means the energy of the graphene supported polyoxometalates and E_{Pt} is the energy of bare Pt atoms. A negative value corresponds to exothermic adsorption. Propene and H_2 adsorption energies and subsequent hydrogenation reaction barriers are also investigated to understand the reaction kinetics. Adsorption energies are calculated regarding to the references of isolated Pt-polyoxometalate catalyst and H_2 in gas phase. During the reaction pathway explorations, 2D graphene layer is not considered for the convenience of calculations. This is valid because of the weak interaction between Pt-polyoxometalate and the graphene layer. Transition state structures are located by NEB method[74-75] and then refined by DIMER method[76]. At the end of the optimizations, the maximum force residues are smaller than 0.03 eV/ Å and only one imaginary frequency presents.

Supporting information

Characterization of catalysts, hydrogenation of phenylacetylene and 1,3-butadine, structural information of local minima, as well as other experimental and DFT details.

Author information

Corresponding Authors

*sautet@ucla.edu (P. S.)

*ning.yan@nus.edu.sg (N. Y.)

Author Contributions

# These authors contributed equally to this work.

Notes

The authors declare no competing financial interests.

Acknowledgements

References

1.   Munnik, P.; de Jongh, P. E.; de Jong, K. P., Recent Developments in the Synthesis of Supported Catalysts. *Chem. Rev.* **2015,** *115* (14), 6687-6718.
2.   Campbell, C. T., The Energetics of Supported Metal Nanoparticles: Relationships to Sintering Rates and Catalytic Activity. *Acc. Chem. Res.* **2013,** *46* (8), 1712-1719.
3.   Bell, A. T., The impact of nanoscience on heterogeneous catalysis. *Science* **2003,** *299* (5613), 1688-1691.
4.   Herzing, A. A.; Kiely, C. J.; Carley, A. F.; Landon, P.; Hutchings, G. J., Identification of active gold nanoclusters on iron oxide supports for CO oxidation. *Science* **2008,** *321* (5894), 1331-1335.
5.   Fang, J.; Zhang, B.; Yao, Q.; Yang, Y.; Xie, J.; Yan, N., Recent advances in the synthesis and catalytic applications of ligand-protected, atomically precise metal nanoclusters. *Coord. Chem. Rev.* **2016,** *322*, 1-29.
6.   Flytzani-Stephanopoulos, M.; Gates, B. C., Atomically Dispersed Supported Metal Catalysts. *Annual Review of Chemical and Biomolecular Engineering* **2012,** *3* (1), 545-574.

7.   Ding, K.; Gulec, A.; Johnson, A. M.; Schweitzer, N. M.; Stucky, G. D.; Marks, L. D.; Stair, P. C., Identification of active sites in CO oxidation and water-gas shift over supported Pt catalysts. *Science* **2015,** *350* (6257), 189-192.

8.   Wei, H.; Liu, X.; Wang, A.; Zhang, L.; Qiao, B.; Yang, X.; Huang, Y.; Miao, S.; Liu, J.; Zhang, T., FeOx-supported platinum single-atom and pseudo-single-atom catalysts for chemoselective hydrogenation of functionalized nitroarenes. *Nat Commun* **2014,** *5*, 5634.

9.   Lucci, F. R.; Liu, J.; Marcinkowski, M. D.; Yang, M.; Allard, L. F.; Flytzani-Stephanopoulos, M.; Sykes, E. C. H., Selective hydrogenation of 1,3-butadiene on platinum-copper alloys at the single-atom limit. *Nat Commun* **2015,** *6*, 8550.

10.   Yang, S.; Kim, J.; Tak, Y. J.; Soon, A.; Lee, H., Single-Atom Catalyst of Platinum Supported on Titanium Nitride for Selective Electrochemical Reactions. *Angew. Chem. Int. Ed.* **2016,** *55* (6), 2058-2062.

11.   Choi, C. H.; Kim, M.; Kwon, H. C.; Cho, S. J.; Yun, S.; Kim, H.-T.; Mayrhofer, K. J. J.; Kim, H.; Choi, M., Tuning selectivity of electrochemical reactions by atomically dispersed platinum catalyst. *Nat Commun* **2016,** *7*, 10922.

12.   Zhu, C.; Fu, S.; Shi, Q.; Du, D.; Lin, Y., Single-Atom Electrocatalysts. *Angew. Chem. Int. Ed.* **2017,** *56* (45), 13944-13960.

13.   Li, X.; Bi, W.; Zhang, L.; Tao, S.; Chu, W.; Zhang, Q.; Luo, Y.; Wu, C.; Xie, Y., Single-Atom Pt as Co-Catalyst for Enhanced Photocatalytic H2 Evolution. *Adv. Mater.* **2016,** *28* (12), 2427-2431.

14.   Gao, G.; Jiao, Y.; Waclawik, E. R.; Du, A., Single Atom (Pd/Pt) Supported on Graphitic Carbon Nitride as an Efficient Photocatalyst for Visible-Light Reduction of Carbon Dioxide. *J. Am. Chem. Soc.* **2016,** *138* (19), 6292-6297.

15.   Lin, L.; Zhou, W.; Gao, R.; Yao, S.; Zhang, X.; Xu, W.; Zheng, S.; Jiang, Z.; Yu, Q.; Li, Y.-W.; Shi, C.; Wen, X.-D.; Ma, D., Low-temperature hydrogen production from water and methanol using Pt/α-MoC catalysts. *Nature* **2017,** *544* (7648), 80-83.

16.   Ouyang, R.; Liu, J.-X.; Li, W.-X., Atomistic Theory of Ostwald Ripening and Disintegration of Supported Metal Particles under Reaction Conditions. *J. Am. Chem. Soc.* **2013,** *135* (5), 1760-1771.

17.   Hansen, T. W.; DeLaRiva, A. T.; Challa, S. R.; Datye, A. K., Sintering of Catalytic Nanoparticles: Particle Migration or Ostwald Ripening? *Acc. Chem. Res.* **2013,** *46* (8), 1720-1730.

18.   O'Connor, N. J.; Jonayat, A. S. M.; Janik, M. J.; Senftle, T. P., Interaction trends between single metal atoms and oxide supports identified with density functional theory and statistical learning. *Nat. Catal.* **2018**, *1*, 531-539.

19.   Kistler, J. D.; Chotigkrai, N.; Xu, P.; Enderle, B.; Praserthdam, P.; Chen, C. Y.; Browning, N. D.; Gates, B. C., A single-site platinum CO oxidation catalyst in zeolite KLTL: microscopic and spectroscopic determination of the locations of the platinum atoms. *Angew. Chem. Int. Ed. Engl.* **2014,** *53* (34), 8904-8907.

20.   Jones, J.; Xiong, H.; DeLaRiva, A. T.; Peterson, E. J.; Pham, H.; Challa, S. R.; Qi, G.; Oh, S.; Wiebenga, M. H.; Pereira Hernández, X. I.; Wang, Y.; Datye, A. K., Thermally stable single-atom platinum-on-ceria catalysts via atom trapping. *Science* **2016,** *353* (6295), 150-154.

21.   Kale, M. J.; Christopher, P., Utilizing Quantitative in Situ FTIR Spectroscopy To Identify Well-Coordinated Pt Atoms as the Active Site for CO Oxidation on Al2O3-Supported Pt Catalysts. *ACS Catalysis* **2016,** *6* (8), 5599-5609.

22.   Matsubu, J. C.; Yang, V. N.; Christopher, P., Isolated Metal Active Site Concentration and Stability Control Catalytic CO2 Reduction Selectivity. *J. Am. Chem. Soc.* **2015,** *137* (8), 3076-3084.

23.   Lang, R.; Li, T.; Matsumura, D.; Miao, S.; Ren, Y.; Cui, Y.-T.; Tan, Y.; Qiao, B.; Li, L.; Wang, A.; Wang, X.; Zhang, T., Hydroformylation of Olefins by a Rhodium Single-Atom

Catalyst with Activity Comparable to RhCl(PPh3)3. *Angew. Chem. Int. Ed.* **2016,** *128* (52), 16288-16292.

24.   Wang, L.; Zhang, W.; Wang, S.; Gao, Z.; Luo, Z.; Wang, X.; Zeng, R.; Li, A.; Li, H.; Wang, M.; Zheng, X.; Zhu, J.; Zhang, W.; Ma, C.; Si, R.; Zeng, J., Atomic-level insights in optimizing reaction paths for hydroformylation reaction over Rh/CoO single-atom catalyst. *Nat. Commun.* **2016,** *7*, 14036.

25.   Yang, M.; Li, S.; Wang, Y.; Herron, J. A.; Xu, Y.; Allard, L. F.; Lee, S.; Huang, J.; Mavrikakis, M.; Flytzani-Stephanopoulos, M., Catalytically active Au-O(OH)x- species stabilized by alkali ions on zeolites and mesoporous oxides. *Science* **2014,** *346* (6216), 1498-1501.

26.   Flytzani-Stephanopoulos, M., Gold Atoms Stabilized on Various Supports Catalyze the Water–Gas Shift Reaction. *Acc. Chem. Res.* **2014,** *47* (3), 783-792.

27.   Duarte, R. B.; Krumeich, F.; van Bokhoven, J. A., Structure, Activity, and Stability of Atomically Dispersed Rh in Methane Steam Reforming. *ACS Catalysis* **2014,** *4* (5), 1279-1286.

28.   Huang, W.; Zhang, S.; Tang, Y.; Li, Y.; Nguyen, L.; Li, Y.; Shan, J.; Xiao, D.; Gagne, R.; Frenkel, A. I.; Tao, F., Low-Temperature Transformation of Methane to Methanol on Pd1O4 Single Sites Anchored on the Internal Surface of Microporous Silicate. *Angew. Chem. Int. Ed.* **2016,** *55* (43), 13441-13445.

29.   Zhang, X.; Sun, Z.; Wang, B.; Tang, Y.; Nguyen, L.; Li, Y.; Tao, F. F., C–C Coupling on Single-Atom-Based Heterogeneous Catalyst. *J. Am. Chem. Soc.* **2018,** *140* (3), 954-962.

30.   Chen, Z.; Vorobyeva, E.; Mitchell, S.; Fako, E.; Ortuño, M. A.; López, N.; Collins, S. M.; Midgley, P. A.; Richard, S.; Vilé, G.; Pérez-Ramírez, J., A heterogeneous single-atom palladium catalyst surpassing homogeneous systems for Suzuki coupling. *Nat. Nanotechnol.* **2018**, 13, 702-707.

31.   Zhang, L.; Wang, A.; Miller, J. T.; Liu, X.; Yang, X.; Wang, W.; Li, L.; Huang, Y.; Mou, C.-Y.; Zhang, T., Efficient and Durable Au Alloyed Pd Single-Atom Catalyst for the Ullmann Reaction of Aryl Chlorides in Water. *ACS Catalysis* **2014,** *4* (5), 1546-1553.

32.   Feng, Q.; Zhao, S.; Wang, Y.; Dong, J.; Chen, W.; He, D.; Wang, D.; Yang, J.; Zhu, Y.; Zhu, H.; Gu, L.; Li, Z.; Liu, Y.; Yu, R.; Li, J.; Li, Y., Isolated Single-Atom Pd Sites in Intermetallic Nanostructures: High Catalytic Selectivity for Semihydrogenation of Alkynes. *J. Am. Chem. Soc.* **2017,** *139* (21), 7294-7301.

33.   Wang, L.; Zhang, S.; Zhu, Y.; Patlolla, A.; Shan, J.; Yoshida, H.; Takeda, S.; Frenkel, A. I.; Tao, F., Catalysis and In Situ Studies of Rh1/Co3O4 Nanorods in Reduction of NO with H2. *ACS Catalysis* **2013,** *3* (5), 1011-1019.

34.   He, P.; Xu, B.; Xu, X.; Song, L.; Wang, X., Surfactant encapsulated palladium-polyoxometalates: controlled assembly and their application as single-atom catalysts. *Chemical Science* **2016,** *7* (2), 1011-1015.

35.   Tian, S.; Wang, Z.; Gong, W.; Chen, W.; Feng, Q.; Xu, Q.; Chen, C.; Chen, C.; Peng, Q.; Gu, L.; Zhao, H.; Hu, P.; Wang, D.; Li, Y., Temperature-Controlled Selectivity of Hydrogenation and Hydrodeoxygenation in the Conversion of Biomass Molecule by the Ru1/mpg-C3N4 Catalyst. *J. Am. Chem. Soc.* **2018,** *140* (36), 11161-11164.

36.   Liu, P.; Zhao, Y.; Qin, R.; Mo, S.; Chen, G.; Gu, L.; Chevrier, D. M.; Zhang, P.; Guo, Q.; Zang, D.; Wu, B.; Fu, G.; Zheng, N., Photochemical route for synthesizing atomically dispersed palladium catalysts. *Science* **2016,** *352* (6287), 797-800.

37.   Yan, H.; Cheng, H.; Yi, H.; Lin, Y.; Yao, T.; Wang, C.; Li, J.; Wei, S.; Lu, J., Single-Atom Pd1/Graphene Catalyst Achieved by Atomic Layer Deposition: Remarkable Performance in Selective Hydrogenation of 1,3-Butadiene. *J. Am. Chem. Soc.* **2015,** *137* (33), 10484-10487.

38.   Vilé, G.; Albani, D.; Nachtegaal, M.; Chen, Z.; Dontsova, D.; Antonietti, M.; López, N.; Pérez-Ramírez, J., A Stable Single-Site Palladium Catalyst for Hydrogenations. *Angew. Chem. Int. Ed.* **2015,** *54* (38), 11265-11269.

39.   Zhang, Z.; Zhu, Y.; Asakura, H.; Zhang, B.; Zhang, J.; Zhou, M.; Han, Y.; Tanaka, T.; Wang, A.; Zhang, T.; Yan, N., Thermally stable single atom Pt/m-Al2O3 for selective hydrogenation and CO oxidation. *Nat Commun* **2017,** *8*, 16100.

40.   Crampton, A. S.; Rötzer, M. D.; Ridge, C. J.; Schweinberger, F. F.; Heiz, U.; Yoon, B.; Landman, U., Structure sensitivity in the nonscalable regime explored via catalysed ethylene hydrogenation on supported platinum nanoclusters. *Nature Communications* **2016,** *7*, 10389.

41.   Zhou, C.; Wu, J.; Nie, A.; Forrey, R. C.; Tachibana, A.; Cheng, H., On the Sequential Hydrogen Dissociative Chemisorption on Small Platinum Clusters: A Density Functional Theory Study. *The Journal of Physical Chemistry C* **2007,** *111* (34), 12773-12778.

42.   Darling, G. R.; Holloway, S., The dissociation of diatomic molecules at surfaces. *Rep. Prog. Phys.* **1995,** *58* (12), 1595.

43.   Spreafico, C.; Karim, W.; Ekinci, Y.; van Bokhoven, J. A.; VandeVondele, J., Hydrogen Adsorption on Nanosized Platinum and Dynamics of Spillover onto Alumina and Titania. *The Journal of Physical Chemistry C* **2017,** *121* (33), 17862-17872.

44.   Esteruelas, M. A.; Oro, L. A., Dihydrogen Complexes as Homogeneous Reduction Catalysts. *Chem. Rev.* **1998,** *98* (2), 577-588.

45.   Zhang, B.; Asakura, H.; Zhang, J.; Zhang, J.; De, S.; Yan, N., Stabilizing a Platinum1 Single-Atom Catalyst on Supported Phosphomolybdic Acid without Compromising Hydrogenation Activity. *Angew. Chem. Int. Ed.* **2016,** *55* (29), 8319-8323.

46.   Zhang, B.; Asakura, H.; Yan, N., Atomically Dispersed Rhodium on Self-Assembled Phosphotungstic Acid: Structural Features and Catalytic CO Oxidation Properties. *Ind. Eng. Chem. Res.* **2017,** *56* (13), 3578-3587.

47.   Liu, C.-G.; Jiang, M.-X.; Su, Z.-M., Computational Study on M1/POM Single-Atom Catalysts (M = Cu, Zn, Ag, and Au; POM = [PW12O40]3–): Metal–Support Interactions and Catalytic Cycle for Alkene Epoxidation. *Inorg. Chem.* **2017**, 56(17), 10496-10504.

48.   Brandts, J. A. M.; Berben, P. H., Application of Immobilized Rhodium Catalyst Precursors in Enantio- and Chemoselective Hydrogenation Reactions. *Organic Process Research & Development* **2003,** *7* (3), 393-398.

49.   Rosario Torviso, M.; Blanco, M. N.; Cáceres, C. V.; Fraile, J. M.; Mayoral, J. A., Supported heteropolyanions as solid counterions for the electrostatic immobilization of chiral copper complexes. *J. Catal.* **2010,** *275* (1), 70-77.

50.   Tanielyan, S. K.; Augustine, R. L.; Marin, N.; Alvez, G., Anchored Wilkinson Catalyst. *ACS Catalysis* **2011,** *1* (2), 159-169.

51.   Ahn, S.-H.; Choi, M.-S.; Im, J.-S.; Sheikh, R.; Park, Y.-H., Improved method for immobilization of a chiral complex on PTA/alumina for asymmetric hydrogenation of a β-ketoester. *J. Mol. Catal. A: Chem.* **2013,** *373*, 55-60.

52.   Tanielyan, S.; Biunno, N.; Bhagat, R.; Augustine, R., Anchored Wilkinson Catalyst: Hydrogenation of β Pinene. *Top. Catal.* **2014,** *57* (17), 1564-1569.

53.   Smolentsev, N.; Sikora, M.; Soldatov, A. V.; Kvashnina, K. O.; Glatzel, P., Spin-orbit sensitive hard x-ray probe of the occupied and unoccupied $5d$ density of states. *Physical Review B* **2011,** *84* (23), 235113.

54.   Moses-DeBusk, M.; Yoon, M.; Allard, L. F.; Mullins, D. R.; Wu, Z.; Yang, X.; Veith, G.; Stocks, G. M.; Narula, C. K., CO Oxidation on Supported Single Pt Atoms: Experimental and ab Initio Density Functional Studies of CO Interaction with Pt Atom on θ-Al2O3(010) Surface. *J. Am. Chem. Soc.* **2013,** *135* (34), 12634-12645.

55.   Molder, J.; Sickle, W.; Sobol, P.; Bomben, K., *Handbook of X-ray Photoelectron Spectroscopy*. Perkin-Elmer Corporation: Eden Prairie, MN: 1992.

56.   Augustine, R. L.; Tanielyan, S. K.; Mahata, N.; Gao, Y.; Zsigmond, A.; Yang, H., Anchored homogeneous catalysts: the role of the heteropoly acid anchoring agent. *Applied Catalysis A: General* **2003,** *256* (1–2), 69-76.

57.   Hülsey, M. J.; Zhang, J.; Yan, N., Harnessing the Wisdom in Colloidal Chemistry to Make Stable Single-Atom Catalysts. *Adv. Mater.* **2018,** *30* (47), 1802304.

58.   Klonowski, P.; Goloboy, J. C.; Uribe-Romo, F. J.; Sun, F.; Zhu, L.; Gándara, F.; Wills, C.; Errington, R. J.; Yaghi, O. M.; Klemperer, W. G., Synthesis and Characterization of the Platinum-Substituted Keggin Anion α-H2SiPtW11O404–. *Inorg. Chem.* **2014,** *53* (24), 13239-13246.

59.   Janthon, P.; Luo, S.; Kozlov, S. M.; Viñes, F.; Limtrakul, J.; Truhlar, D. G.; Illas, F., Bulk Properties of Transition Metals: A Challenge for the Design of Universal Density Functionals. *J. Chem. Theory Comput.* **2014,** *10* (9), 3832-3839.

60.   Wang, A.; Li, J.; Zhang, T., Heterogeneous single-atom catalysis. *Nature Reviews Chemistry* **2018,** *2* (6), 65-81.

61.   Naumann d'Alnoncourt, R.; Friedrich, M.; Kunkes, E.; Rosenthal, D.; Girgsdies, F.; Zhang, B.; Shao, L.; Schuster, M.; Behrens, M.; Schlögl, R., Strong metal–support interactions between palladium and iron oxide and their effect on CO oxidation. *J. Catal.* **2014,** *317*, 220-228.

62.   Gautier, S.; Steinmann, S. N.; Michel, C.; Fleurat-Lessard, P.; Sautet, P., Molecular adsorption at Pt(111). How accurate are DFT functionals? *PCCP* **2015,** *17* (43), 28921-28930.

63.   Chen, Y.; Vlachos, D. G., Hydrogenation of Ethylene and Dehydrogenation and Hydrogenolysis of Ethane on Pt(111) and Pt(211): A Density Functional Theory Study. *The Journal of Physical Chemistry C* **2010,** *114* (11), 4973-4982.

64.   Cremer, P. S.; Su, X.; Shen, Y. R.; Somorjai, G. A., Ethylene Hydrogenation on Pt(111) Monitored in Situ at High Pressures Using Sum Frequency Generation. *J. Am. Chem. Soc.* **1996,** *118* (12), 2942-2949.

65.   Bond, G. C.; Keane, M. A.; Kral, H.; Lercher, J. A., Compensation Phenomena in Heterogeneous Catalysis: General Principles and a Possible Explanation. *Catalysis Reviews* **2000,** *42* (3), 323-383.

66.   Roduner, E., Understanding catalysis. *Chem. Soc. Rev.* **2014,** *43* (24), 8226-8239.

67.   Mager-Maury, C.; Bonnard, G.; Chizallet, C.; Sautet, P.; Raybaud, P., H2-Induced Reconstruction of Supported Pt Clusters: Metal–Support Interaction versus Surface Hydride. *ChemCatChem* **2011,** *3* (1), 200-207.

68.   Blöchl, P. E., Projector augmented-wave method. *Physical Review B* **1994,** *50* (24), 17953-17979.

69.   Kresse, G.; Joubert, D., From ultrasoft pseudopotentials to the projector augmented-wave method. *Physical Review B* **1999,** *59* (3), 1758-1775.

70.   Perdew, J. P.; Burke, K.; Ernzerhof, M., Generalized Gradient Approximation Made Simple. *Phys. Rev. Lett.* **1996,** *77* (18), 3865-3868.

71.   Zhang, Y.; Tsu, R., Binding Graphene Sheets Together Using Silicon: Graphene/Silicon Superlattice. *Nanoscale Research Letters* **2010,** *5* (5), 805-808.

72.   Wen, S.; Guan, W.; Kan, Y.; Yang, G.; Ma, N.; Yan, L.; Su, Z.; Chen, G., Theoretical insights into [PMo12O40]3- grafted on single-walled carbon nanotubes. *PCCP* **2013,** *15* (23), 9177-9185.

73.   Wen, S.; Guan, W.; Wang, J.; Lang, Z.; Yan, L.; Su, Z., Theoretical investigation of structural and electronic propertyies of [PW12O40]3- on graphene layer. *Dalton Transactions* **2012,** *41* (15), 4602-4607.

74.   Henkelman, G.; Uberuaga, B. P.; Jónsson, H., A climbing image nudged elastic band method for finding saddle points and minimum energy paths. *J. Chem. Phys.* **2000,** *113* (22), 9901-9904.

75.   Henkelman, G.; Jónsson, H., Improved tangent estimate in the nudged elastic band method for finding minimum energy paths and saddle points. *J. Chem. Phys.* **2000,** *113* (22), 9978-9985.

76.   Henkelman, G.; Jónsson, H., A dimer method for finding saddle points on high dimensional potential surfaces using only first derivatives. *J. Chem. Phys.* **1999,** *111* (15), 7010-7022.